polymers

MDPI

Article

Time-Resolved Radiation-Induced Conductivity of Polyimide and Its Description Using the Multiple Trapping Formalism

Andrey Tyutnev, Vladimir Saenko *, Aleksei Zhadov and Evgenii Pozhidaev

National Research University Higher School of Economics, Moscow 101000, Russia; aptyutnev@yandex.ru (A.T.); exfaust@yandex.ru (A.Z.); epozhidaev@hse.ru (E.P.)

* Correspondence: saenko19@gmail.com or vsaenko@hse.ru

Received: 1 November 2019; Accepted: 8 December 2019; Published: 11 December 2019

Abstract: Polymer dielectrics subjected to intense radiation fluxes exhibit a radiation-induced conductivity (RIC). Polyimide is a good dielectric with excellent mechanical and thermal properties featuring high radiation resistance currently widely used in the spacecraft industry. Its RIC has been extensively studied in several laboratories. The purpose of the present study is to make a direct measurement of the RIC for both pulsed and continuous irradiation using a current sensing technique, which is contrary to the indirect method employing a surface-potential decay technique that is now preferred by spacecraft charging engineers. Our experiments are done in a small-signal regime excluding any recombination and dose effects. In combination with existing computer codes, we managed to develop further the conventional multiple trapping formalism and the RIC theory based on it. The main idea is to supplement an exponential trap distribution responsible for a dominant dispersive carrier transport in polymers with a small concentration of inherent deep traps which may or may not have an energy distribution. In line with this reasoning, we propose a tentative set of RIC model parameters for polyimide that accounts for the observed experimental data. The findings and their implications are discussed in a broad context of previous studies.

Keywords: polymers; irradiation by electrons; small-signal regime; dispersive transport; numerical calculations

1. Introduction

The radiation-induced conductivity (RIC) in insulators (polymers included) refers to an additional conductivity in excess of their dark one when subjected to intense radiation fluxes. RIC studies in polymers have a long and fortuitous history dating back to 1956 [1] and, from the very beginning, used an approach first suggested by Rose in 1953 [2], which later became known as a quasi-band multiple trapping (MT) formalism [3,4]. In it, charge carriers (electrons and holes) generated by an ionizing radiation emerge in a conducting state. Their lifetime in this state is only too short, due to the presence of numerous traps distributed exponentially in the binding energy. Trapped carriers can be thermally de-trapped into the conduction zone to be re-captured immediately again. This chain of events continues until a carrier recombines or exits a sample. Hence the name of this type of carrier transport in polymers—the multiple trapping model (MTM). The MTM successfully described such different phenomena as the current injection in solids [5], thermally stimulated currents (glow curves) in irradiated polymers [6], and the time of flight (TOF) results in photoconductive organic materials (molecularly doped polymers included) [7,8]. It was only natural to base the RIC theory on the MTM formalism. The famous Rose-Fowler-Vaisberg (RFV) model fully incorporated it from the very beginning in 1982 [9]. Four years later, we developed a powerful computer code to numerically

solve the RFV equations relating to the step-function uniform irradiation of an infinite polymer slab with the carrier balance being governed by the bimolecular recombination only [10]. Subsequently, this code has been extended to the case of a finite slab with the carrier exit to electrodes controlling the process [11]. These numerical codes allowed to overcome the main limitation inherent to analytical solutions, including closed-form ones [12], which required that the dispersion parameter be was less than 0.5.

All this time, leading research groups (Gross et al. [13,14], and currently French researchers [15]) adhered to the two-trap RIC model whose parameters were retrieved from experiments which were not intended to directly measure the RIC itself (this last approach was again first proposed by Gross [16,17]). In this respect, one should remember Hughes as an eager proponent of advanced ideas that were intensively developed in the radiation chemistry of organic solids and in the area of the charge carrier transport in photoconductive polymers (see review [18]). In this context, the paper [19] coauthored by Hughes deserves special attention. Published in 1983, it went mostly unnoticed by the RIC community. However, recently it initiated a hot debate [20] which led to the extension of the conventional RFV model, which is analyzed in the present work.

As our modified RFV model is only at the development stage, it needs a most accurate disposition of experimental details of data acquisition, their processing, and interpretation assisted by numerical calculations to find model parameters that fit the RIC results.

2. Materials, Methods, and Problem Formulation

2.1. Materials

For our studies, we used commercial films of Russian-made polyimide (trademark PM-1), which is, polypyromelliteimide containing proprietary additives. This polymer may be considered as an analog of Kapton (DuPont, Wilmington, DE, USA). We investigated its RIC for quite a long time (see [21]). PM-1 films had a thickness of 12 μm and samples cut from this film were 40 mm in diameter. Al electrodes (about 50 nm thick and 32 mm in diameter) were thermally evaporated on opposite sample sides in vacuum.

2.2. Methods

Figure 1 gives a schematic representation of the experimental setup used in this study.

To irradiate the polymer samples, we employed 50-keV electrons supplied by an electron gun ELA-65. The experimental setup used in the present study was recently described in our latest works [20,21]. Here, we present a detailed description of it.

Beam electrons pass through a collimator (20 mm in diameter) bombarding a test sample to form an irradiation spot 30 mm in diameter. Between the collimator and the sample there is an Al shutter covered with an electroluminescent conducting paint. The shutter serves two purposes. First, it is used to not only to control an electron current after preliminarily calibrating it against a Faraday cup but also to visualize the current surface uniformity. Second, the shutter allows starting and terminating the continuous irradiation with an opening time 0.08 s.

The electron current density was found to be constant to within 5% when measured over the entire irradiated surface. This finding was verified by registering an electron current by a shutter for some time and observing for current variations. They did not exceed the claimed 5% stability. The dose depth deposition was rather non-uniform in line with literature data (see for example [22]). Evidently, this is a problem for RIC assessment and methods to circumvent it, and this will be discussed below.

The pulse duration was fixed at 20 μs and 1 ms, with typical rise and fall times at 0.7 and 10 μs, respectively. During the main part of the irradiation run (both pulsed and continuous) an electron current density was essentially constant, thus imitating a step-function dose rate profile. Furthermore, we used a small-signal irradiation regime as much as possible (violation of this rule is clearly noted).

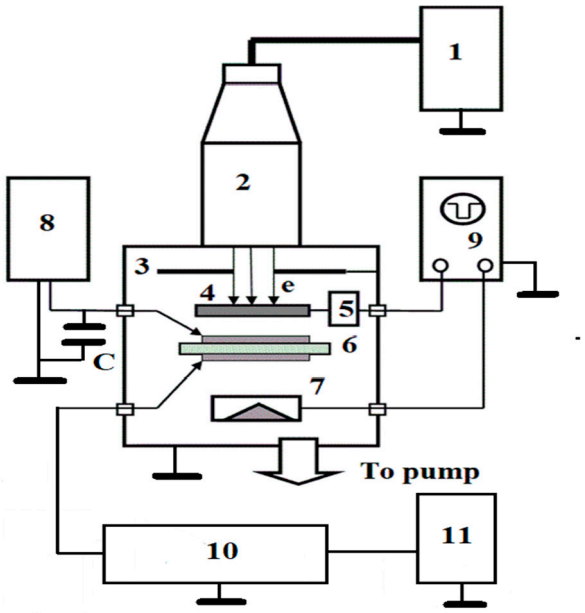

Figure 1. Schematic representation of the experimental setup for measuring polymer RIC in pulsed and continuous regimes. 1—high-voltage power supply; 2—electron gun; 3—electron beam collimator; 4—metallic shutter; 5—shutter control system; 6—test sample with evaporated Al electrodes; 7—Faraday cup; 8—DC voltage supply with an accumulative capacitor C and an electric circuit to put on and off the output voltage and control it; 9—double-beam Tektronix 3012B oscilloscope with a bandwidth of 300 MHz, 10—electronic block for measuring an analog RIC signal, amplifying and analog-to-digital converting and finally sending the ORIGIN current curve to printer 11.

The test sample was a part of a series electrical circuit consisting of a voltage source (up to 1200 V) and a load resistor (Figure 2). The voltage drop over this resistor allowed determining the current passing through the sample. As in [20,21], to facilitate data reduction, this voltage drop was amplified, converted from the analog to digital format, put into a PC computer to be processed by the Origin program and finally stored for future use. When necessary, Origin files could be printed immediately.

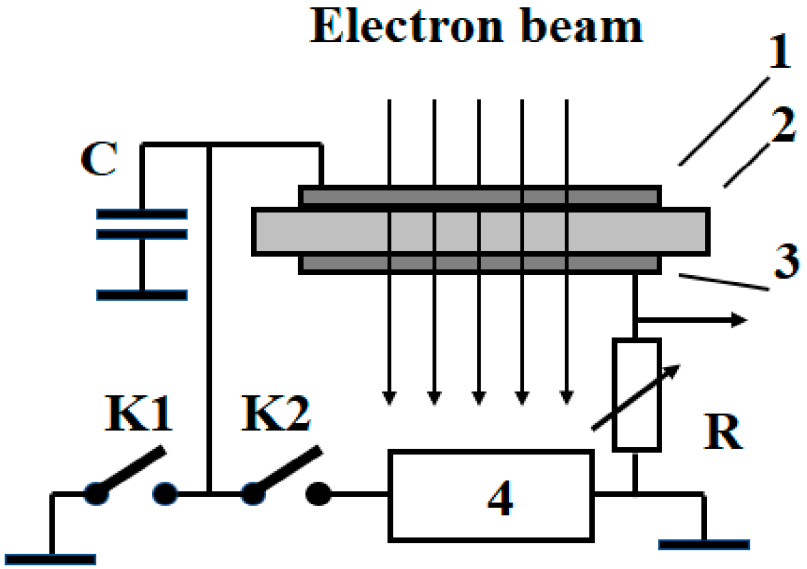

Figure 2. Schematic representation of the measuring setup. 1—potential electrode; 2—test sample; 3—measuring electrode; 4—voltage source. C is an accumulative capacitor as in Figure 1; K1 and K2 are switches (when one is open, the other is automatically closed); R is a load (measuring) resistor.

But only part of this current defines the RIC proper, the other contributions come from the displacement (polarization) current and the radiation-driven current arising from specifics of the fast electron transport in a solid medium. The conventional description of the radiation-driven currents was given by Gross et al. [16] using a newly developed split Faraday cup technique. It was shown that some of the primary and secondary electrons stop inside a sample and cause a current to flow in the closed circuit even in the absence of the voltage source. It is important that the magnitude of the radiation-driven current is not affected by the applied voltage (in our experiments, less than 1200 V).

Measuring Method

First, we put an electron gun into an operational condition for an intended experiment and determined the radiation-driven current i_{rd} irradiating a sample with no applied voltage (switch K1 closed and switch K2 open) by a few pulses or alternatively, subjecting it to a continuous irradiation for a short period of time.

Second, the shutter blocking the beam and switches being put in reversed positions (switch K1 open and switch K2 closed), the voltage was now applied for a few minutes, allowing a displacement (polarization) current to die out, which is easily achieved since PI is an excellent dielectric. This way, one gets rid of the displacement current even for continuous irradiations at the smallest dose rates used (see Figure 5, the star-marked curve) when conductivity under irradiation ($\sim 10^{-13}$ Ω^{-1} m^{-1}) is much greater than the PI dark conductivity (about 10^{-16} $\Omega^{-1}m^{-1}$). After the depolarization procedure was over, we resumed an experimental run proper by putting off the shutter.

To find the current $i_r(t)$ directly associated with the RIC, one has to subtract algebraically the previously determined i_{rd} from the measured total current $i_{rt}(t)$ passing through the poled sample under irradiation (as mentioned earlier, a displacement current is negligibly small). Once we know the RIC current i_r, the applied voltage V, the area of the irradiated spot S, and the film thickness L, the radiation-induced conductivity γ_r can be assessed in a straightforward way:

$$\gamma_r(t) = i_r(t)L/VS \tag{1}$$

The final aim of the experiment is to correlate the temporal dependence of γ_r with the relevant dose rate R_0. To find it, we rely on our previous experimental and numerical (Monte-Carlo) simulations [21]. The best approach is to identify R_0 with the dose rate averaged over a sample thickness. For a current 100 nA measured by the shutter, it was estimated to be 190 Gy/s. Dose rate non-uniformity was ±30%. The minimum dose rate for continuous irradiation was 0.3 Gy/s and is limited by the beam current instability and the rf-noise in the measuring circuit.

In time-of-flight (TOF) experiments, the notion of the radiation-induced conductivity γ_r becomes meaningless, so one introduces a current density $j_r(t) = i_r(t)/S$ as the main output quantity.

Irradiations have been done in vacuum (approximately 10^{-3} Pa) at room temperature only. Most experiments used fresh (pristine) samples especially for continuous irradiations.

2.3. Problem Formulation

The interpretation of RIC results relies heavily on the nature of RIC phenomenon, multiple trapping formalism (dispersive transport of charge carriers), and the fundamental theories from the radiation chemistry of organic solids (an ion-pair radiolysis, the Onsager theory of the free carrier generation and the geminate conductivity) [23].

Because 50-keV electrons, like gamma- and X-rays, have a low energy transfer rate, they produce geminate ion pairs randomly in irradiated volume. For observation times exceeding some microseconds, geminate pairs have enough time to complete the initial recombination and emerge as separated electron-hole pairs in accordance with the Onsager theory [23]. Hence, their subsequent evolution (drift, diffusion and trapping) may be described by rate equations using appropriate kinetic coefficients for recombination, capture, and so forth.

It is known that RIC consists of two components [18]. Prompt one accounts for the carrier drift before trapping, while the delayed component is due to all carriers which experienced thermal de-trapping if only once: $\gamma_r = \gamma_p + \gamma_d$. At present, it is the general consensus that

$$\gamma_p = K_p R_0, \tag{2}$$

where K_p is an empirical coefficient independent of an electric field and, partly, of temperature [18]. We estimated it using a triangular pulse with the full width at half maximum 1.5 μs: $K_p = 1.5 \times 10^{-15}$ Ω $^{-1}$m^{-1}Gy^{-1}s. Test conditions are as follows: dose rate 2×10^5 Gy/s, dose per pulse 0.35 Gy, electric field 5 V/μm) were enough to secure clear predominance of the prompt component over the delayed one. At longer pulses and stronger electric fields the opposite situation occurs. Hence, model parameters should be found by fitting experimental and numerical current curves relating to the RIC delayed components (below, RICd curves). The difference between RIC and RICd curves concerns not only their values but build-up shapes as well (compare curves (1) and (1a) in Figure 3a).

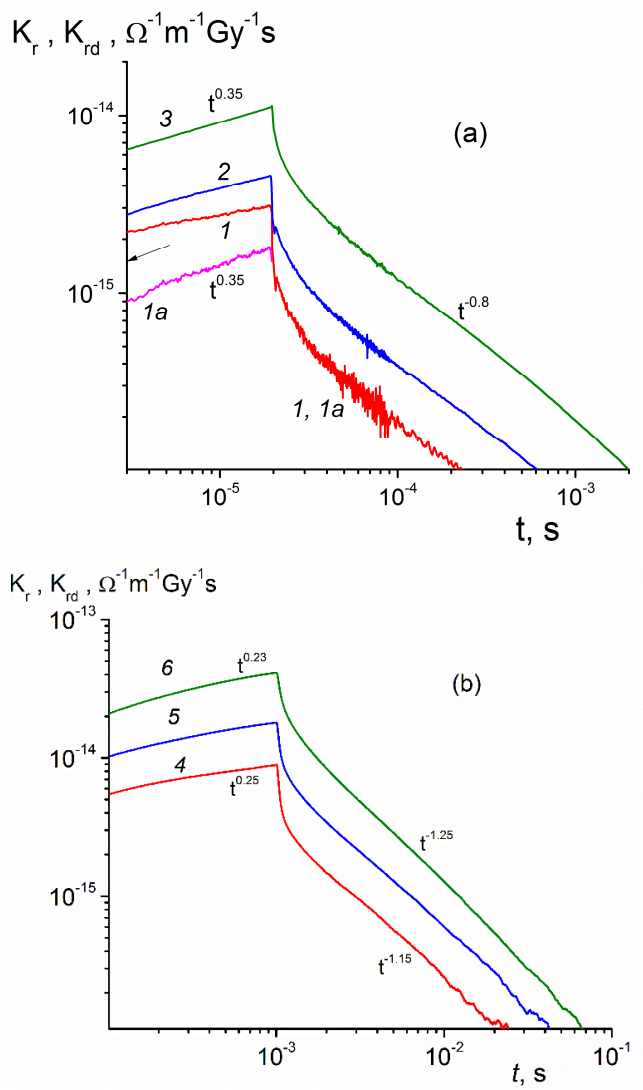

Figure 3. Normalized RIC (K_r) and RICd (K_{rd}) curves (*1*–*6*) and (*1a*), respectively. Pulse length 20 μs (Figure 3a, curves (*1*–*3*) and 1 ms (Figure 3b, curves (*4*–*6*). Electric field: 20 (1, 1a, 4), 40 (2, *5*) and 80 V/μm (3, 6), small-signal irradiation regime. Normalized prompt conductivity $K_p = \gamma_p / R_0 = 1.3 \times 10^{-15}$ Ω $^{-1}$m^{-1}Gy^{-1}s is indicated by an arrow in Figure 3a.

As a prototype RIC model, we consider the modified RFV (RFVm) recently proposed in our paper [20]. The rate equations of this model are as follows:

$$\partial\rho/\partial t = (N_0/\tau_0)[M(E) - \rho]/M_0 - \rho\nu_0 \exp(-\frac{E}{kT}) \tag{3}$$

$$N = N_0 + \int_0^\infty \rho dE \tag{4}$$

$$dN/dt = g_0 - k_{rec}N_0N \tag{5}$$

It is seen that this is a purely time-dependent Cauchy-type problem. The first two equations are conventional in MT formalism, the last one accounts for the effect of a bimolecular recombination. Now, N is the total concentration of the mobile carriers (in our case, holes). Due to the charge neutrality, the total concentrations of holes and electrons (immobile carriers being recombination centers) are equal at any moment of time. N_0 is their concentration in the conduction zone where they have microscopic mobility μ_0 and lifetime τ_0. The energy trap distribution is $M(E)$, with the total trap concentration being M_0 (note, trap energy is taken to be positive). The distribution function of trapped carriers is given by $\rho(E)$. Furthermore, ν_0 is the frequency factor, T—temperature, k—the Boltzmann constant, g_0—the generation rate of the separated electron-hole pairs (during irradiation constant) and k_{rec}—recombination constant. Now, we have to specify the trap distribution as a function of energy. The conventional RFV model uses in this case a simple exponential [18]

$$M(E) = \frac{M_0}{E_1} \exp(-E/E_1), \tag{6}$$

where E_1 is, in fact, an average trap energy. Dispersion parameter $\alpha = kT/E_1$ controls RIC current shapes for step-function irradiation in a small-signal regime. As mentioned earlier, for $\alpha \leq 0.5$ there are even closed-form expressions for these current shapes [12]. In a modified RFV model, the above trap distribution extends only to the separation energy E_s. For $E \geq E_s$ the distribution parameter of this exponential E_2 appreciably rises. Now, we have to deal with two dispersion parameters: α_1 (the former α) and $\alpha_2 = kT/E_2$. The idea of this separation is that each of the two trap fractions clearly identifies its contribution to the RIC, as suggested in [20]. An explicit form of $M(E)$ is as follows

$$\begin{aligned} M(E) &= \tfrac{\hat{M}_0}{E_1} \exp(-E/E_1),\ E < E_s \\ M(E) &= \tfrac{\hat{M}_0}{E_1} \exp(-E_s/E_1) \exp[(E - E_s)/E_2],\ E \geq E_s, \end{aligned} \tag{7}$$

where $\hat{M}_0 = M_0\left[1 + (\frac{E_2}{E_1} - 1) \exp(-E_s/E_1)\right]^{-1}$.

For reference, we indicate that the relative fraction of deep traps is equal to

$$\eta = M_2/M_0 = \frac{(E_2/E_1) \exp(-E_s/E_1)}{1 + (E_2/E_1 - 1) \exp(-E_s/E_1)} \tag{8}$$

and for $\exp(-E_s/E_1) \ll 1$ we have

$$\eta \approx \frac{E_2}{E_1} \exp(-E_s/E_1). \tag{9}$$

Here, M_2 is the concentration of deep traps with energies exceeding E_s.

One note of caution. In the framework of the RFVm, the RIC prompt component $\widehat{\gamma}_p = g_0\mu_0\tau_0 e$ (e is an electronic charge) is a field dependent quantity that duplicates the field dependence of g_0 contrary to the genuine RIC prompt conductivity which is field independent.

3. Results

The most unambiguous information is provided by the RIC current curves relating to 20 μs square pulses (Figure 3a). We plot RIC and RICd data as conductivities reduced to a unit dose rate, namely K_r and K_{rd}, in line with the reduced prompt conductivity (see Equation (2)). This procedure is quite legitimate for small-signal irradiations when both conductivities scale with the dose rate. However, unlike K_p, which is a constant, K_r and K_{rd} depend explicitly on time and parametrically on the electric field.

Let us concentrate on curves (*1*) and (*1a*). They serve to illustrate vividly the situation with the characterization of such curves. Note that they are plotted on a logarithmic scale to produce prolong straight lines whose slopes $\beta = d\lg K/d\lg t$ (positive) near the pulse end or in an asymptotic decay region (usually longer than 3 or 4 pulse lengths) $\beta_1 = -\beta$ (also positive) seem to be appropriate characterization parameters. We designate β_r and β_d for RIC and RICd curves, respectively. These slopes are indicated near curves as t^{β_r,β_d} or $t^{-\beta_1}$.

To characterize curves qualitatively, we indicate K_r and K_{rd} values at the pulse end. For example, for curve 1 β_r is 0.16 and for curve 1a β_d is 0.35 while β_1 is 0.8 for both curves with K_{rd} (20 μs) = 1.7×10^{-15} $\Omega^{-1}\text{m}^{-1}\text{Gy}^{-1}\text{s}$. The value $\beta_d = 0.35$ for curve *1a* is surely to be associated with the dispersion parameter α_1.

All these figures refer to an electric field 20 V/μm. It is remarkable that β_d and β_1 stay unvaried as the field rises four times, which means that an important property is being captured by analyzing the RICd and not the total RIC producing unstable behavior. As expected, K_{rd} (20 μs) steadily rises with field approximately as a power law $K_{rd} \propto F_0^{\delta}$ and $\delta \approx 1.1$.

Figure 3b relating to 1 ms shows that these data are less exemplary, as β_1 is slightly unstable but power law $K_{rd} \propto F_0^{\delta}$ still holds. What is important is that β_d drops to 0.24 for this pulse and this happens irrespective of an electric field. Values of β_1 exceeding unity (1.15 and 1.25), suggestive of the TOF effects, are in effect misleading (see later).

Long-time, step-function irradiations are presently unavailable for the electron gun used. In this situation, we made continuous irradiations registering RIC currents from 0.1 s when a constant beam current was established (Figure 4). Curve *1* was taken at a low dose rate and produced γ_{rd}, rising as $t^{0.12}$ for $t \leq 0.3$ s. This finding shows that β_d continues to decrease as the irradiation time increases.

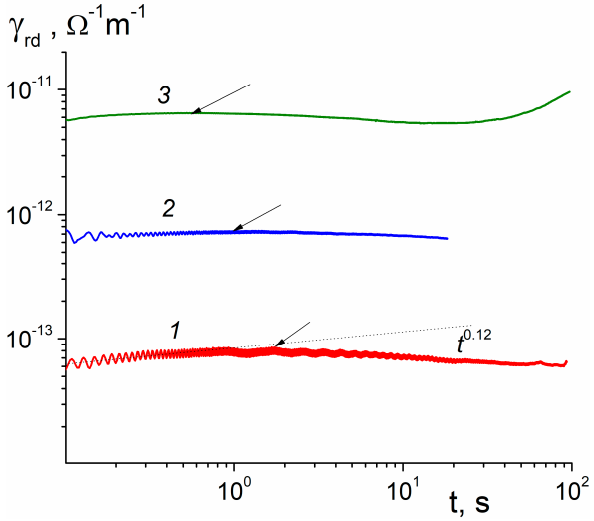

Figure 4. RICd curves for continuous irradiation with dose rate 1.7 (*1*), 17 (*2*), and 170 Gy/s (3). Arrows indicate maximum values of γ_{rd}. Electric field 40 V/μm, small-signal regime is operative only for curve (*1*) and only for $t \leq 0.3$ s.

At still longer times, RICd reaches a maximum at about 1.7 s. Increasing the dose rate (curves *2* and *3*) shifts this time to smaller times, the maximum value rises in accord with a power law $\gamma_{rd} \propto R_0^{\Delta}$

predicted by the conventional RFV model (see [18]). According to this model $\Delta = (1+\alpha)^{-1}$. In our case, α should be evidently replaced with α_2. From Figure 4, we estimated an exponent Δ to be equal to 0.95 leading to $\alpha_2 = 0.05$. Curve *3* starts to rise even further after 20 s of irradiation but such a behavior should be ascribed to a dose effect (the so-called dose-modified RIC [21], whose nature is yet to be understood) and it happens in both PM-1 and Kapton.

Based on our experimental data presented on Figures 3 and 4 for an electric field 40 V/μm, we made a tentative attempt to describe RIC results with the RFVm model using the following model parameters (found by an iteration procedure): $\alpha_1 = 0.4$ ($E_1 = 0.0625$ eV), $\alpha_2 = 0.01$ ($E_2 = 2.5$ eV), $\nu_0 = 10^9$ s^{-1}, $\tau_0 = 10^{-11}$ s, $\mu_0 = 10^{-6}$ m^2/V s, $k_{rec} = 2.4 \times 10^{-14}$ m^{3}s^{-1}, $M_0 = 10^{26}$ m^{-3}, $E_s = 0.55$ eV and $\eta = 0.006$ (according to Formulas (8) and (9)). Now, we have to specify a relationship between R_0 and g_0, allowing the comparison of computed and experimental data. For an electric field 40 V/μm, the radiation yield of free electron-hole pairs may be taken to be 0.7 per 100 eV of absorbed energy (like in polyethylene terephthalate used in [20]). Finally we get the relationship sought: g_0 (m^{-3} s^{-1}) = 6.24×10^{19} R_0 (Gy/s) used in Figure 5, which shows the quality of fit of the numerical calculations to experimental results using the above set of RFVm model parameters.

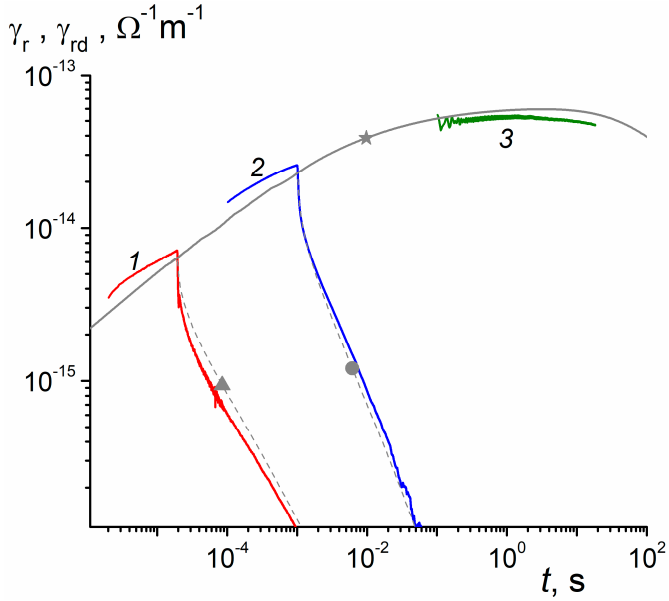

Figure 5. Experimental RIC (*1*–*3*) and computed (indicated by markers) RICd curves. Experimental dose rate 1.6 Gy/s and an equivalent generation rate g_0 used in numerical calculations is 10^{20} m^{-3}s^{-1}. Irradiation time 20 μm (*1*, triangle), 1 ms (*2*, circle), 30 s (*3*), and 100 s (star). RIC curves 1 and 2 are slightly scaled curves 2 and 5 in Figure 3. Electric field is 40 V/μm.

Computed RICd star-marked curve for the long-time irradiation well reproduces the build-up parts of RIC curves. Furthermore, it confirms that slope β_d indeed falls off as irradiation length increases. At about 10 s, curve 4 reaches a maximum, indicating that the bimolecular recombination begins to play a decisive role. Certainly, it interferes with the curve shape already in the sub-second region where the small-signal regime begins to fail. To resolve this ambiguity, we extended numerical calculations of Figure 5 to dose rate extremes (Figure 6).

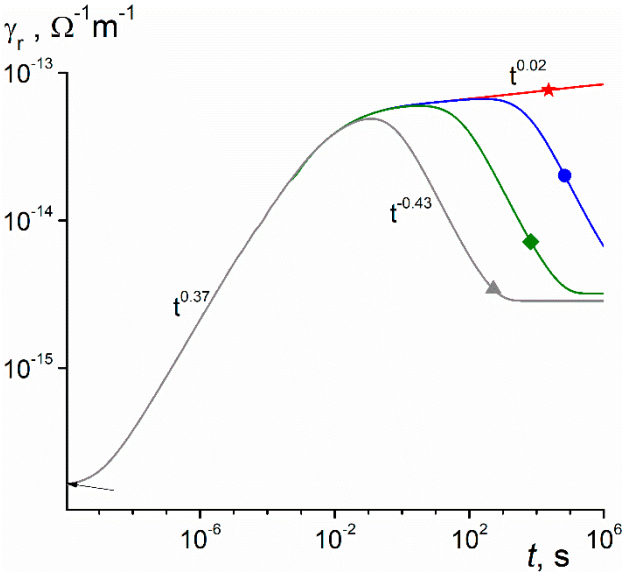

Figure 6. Computed RIC curves scaled by a factor $\xi = 10^{20}$ $m^{-3}s^{-1}/g_0$ to make them to coincide at early times ($t \leq 100$ μs). Generation rate g_0 is 10^{14} (star), 10^{18} (circle), 10^{20} (diamond, unaffected by ξ), and 10^{22} $m^{-3}s^{-1}$ (triangle). The RFVm prompt conductivity is indicated by an arrow and is equal to 1.6×10^{-16} Ω^{-1} m^{-1} for diamond-marked curve. Irradiation time is 10^6 s.

The form of presentation of computed curves in Figure 6 highlights all the important issues under debate. First, a star-marked curve allows to determine accurate values of β_d at early times (from 1 to 100 μs when RICd clearly dominates over prompt conductivity). Its value, 0.37, is slightly smaller than $\alpha_1 = 0.4$ eV but larger than the experimental value 0.35, as Figure 3a shows. Second, the asymptotic value of conductivity rise $\gamma_{rd} \propto t^{0.02}$ (the expected law is $\gamma_{rd} \propto t^{\alpha_2} = t^{0.01}$) slightly fails. Third, a star-curve demonstrates limits of the small-signal irradiations (every curve for $g_0 \leq 10^{14}$ $m^{-3}s^{-1}$ will simply fall on a star-curve). We see that increasing g_0 invariably places respective curves below a star-curve and more so the greater it is. Curve *3* is effectively curve *4* and now it becomes clear that the last curve should be treated as recombination free for times smaller than 0.3 s. Also, β_d for a diamond-curve steadily falls with irradiation time constituting 0.25 at 1 ms, 0.1 at 0.1 s, 0.08 and 0.03 at 1 s, reaching the recombination limited maximum between 3 to 10 s when β_d drops to zero. These data generally agree with the experimental results presented in Figures 3–5.

Processing recombination affected curves in Figure 6 shows that the rad-ampere characteristic looks like an experimental one $\gamma_{rm} \propto g_0^{\Delta}$ (see Figure 4) with $\Delta = 0.95$ in clear contradiction with the expected value $(1 + \alpha_2)^{-1} = 0.99$. However, to detect such small differences in Δ values at long irradiation times presents a real challenge to a researcher. Future work is needed to clarify this ambiguous issue.

4. Discussion

Radiation-induced conductivity of polymers was studied either under pulsed or continuous irradiations. Pulsed studies used bell-shaped pulses not well suited for a detailed kinetic analysis. Researchers had difficulty in separating contributions of the prompt and delayed RIC components. An empirical one- or two-trap model was used to interpret experimental results. No breakthrough information was obtained. Currently, these works are of historical interest only (see [24–27]). This early effort found logical conclusion in our works [9,28]. The last article dealt with pulsed (8, 40 ns and 0.3 ms) RIC data for a broad polymer list reporting values of K_p. Furthermore, for the first time, we proposed an RFV treatment of pulsed irradiations that introduces the notion of the initial effective mobility $\mu_{in} = \frac{\alpha}{1+\alpha}\mu_0\tau_0\nu_0$ [28]. In addition, we developed a simple analytic approach to estimate the frequency factor itself. Finally, using William's approach [29] in combination with μ_{in}, we suggested a simple estimation of the recombination time of the geminate electron-hole pairs that were later

confirmed by numerical simulations [30,31]. Thus, our works [9,28–31] developed a methodology (both experimental and theoretical) for interpreting the RIC pulsed experiments.

As for continuous irradiations, it was a common practice to keep the dose rate constant, thus realizing a near step-function electron-beam (or an X-ray) profile. To avoid the dose effects, experiments were done only on fresh samples. The main information of these early studies was an exponent Δ in a power-like dependence of the steady-state conductivity on dose rate, which usually was less than 1 Gy/s [1] (a list of appropriate references may be found in [32]). Later RIC investigations using intense electron beams (10–1000 Gy/s) clearly demonstrated that there was no RIC steady state. Instead, there was a very slow approach to a maximum. Gross et al. [33] were first to report this result, relying on the two-trap model [33,34]. Our studies confirmed this finding but an explanation has been given using the RFV model [32]. Later, we discovered that the time of RIC maximum (current overshoot) may be substantially lengthened because the bimolecular recombination may become essentially retarded compared to the Langevin mechanism [35]. This phenomenon was called the non-Langevin recombination and was widely reported afterwards [36].

As already mentioned, a two-trap quasi-band model proved very popular in studies of the electron charging of polymer slabs with non-penetrating beams [16,17]. Recently, it found a new lease on life for the interpretation of charging polymer films (used or intended for use) in spacecrafts by electron beams closely imitating the spectra of plasma electrons in Earth orbits [15,37]. The ONERA researchers employed the surface potential decay method sometimes in the presence of fully penetrating electrons with a current density close to real values in orbit. Analyzing these data allows to find the RIC decay curves from which the two-trap model parameters can be retrieved [38–40]. In our opinion, this information should not be directly compared with RFV model parameters in view of discrepancies between RIC data found by potential-decay method and a direct RIC current measuring technique reported in [38]. The model of charge carrier transport in polymer slabs irradiated with non-penetrating electrons has been reviewed in [41].

A two-trap model suffers serious deficiencies if used for analysis of the RIC in polymers. It totally ignores the contribution of the prompt conductivity as well as the multiple trapping type of a charge carrier transport in disordered organics. Hence, this model should be viewed only as an engineering tool for fitting experimental data referring to electron charging phenomena in which the RIC plays an important but yet to be defined role. The RFV model is certainly a step forward in describing RIC in polymers. We applied it to make probe numerical calculations of polymer charging with non-penetrating electrons, as well as bulk charging by substorm electrons of the SCATHA geosynchronous orbit environment [42]. In this respect, one should mention yet another microscopic theory of RIC based on the α-, β-, and γ—relaxations (molecular motions) in polymers (see review by Khatipov [43]). Kinetic equations describing carrier transport are unnecessary cumbersome and lack physical transparency. As a result, it has not been accepted by the RIC community. Our attempt to include effects of molecular motions into the RFV model proved inconclusive as well [44].

After a ten year break devoted to the study of charge carrier transport in molecularly doped or photoconductive polymers (see [18] and our latest papers on the subject [45,46]), we turned our attention back to RIC in polymers [20,21], paying special attention to the small-signal step-function irradiations in both pulsed and continuous regimes [20]. In doing so, we relied heavily on our previous experience in the field. The real problems have started to emerge as soon as we compared pulsed and continuous irradiations of the same polymer samples under identical conditions using a small-signal regime.

The RFV model requires that under these conditions two fundamental relationships hold:

$$\beta_1 = (1 - \alpha) \tag{10}$$

and

$$\Delta = (1 + \alpha)^{-1}, \tag{11}$$

where Δ defines now a dose rate dependence of the maximum radiation-induced conductivity. Both relationships grossly fail in PM-1. Indeed, the dispersion parameter at early times (1 to 20 μs) is about 0.35 (see Figure 3a) which would require $\beta_1 = 0.65$, while its experimental value was between 0.8 and 1.1 (see Figure 3a,b). More to that, an approach of RIC to its maximum should follow a power law $\gamma_{rd} \propto t^{\beta_d}$ with $\beta_d = \alpha$ almost to a maximum itself (Figure 1 in [18]). Experimental value of Δ is 0.95 and according to Equation (11) α is expected to be 0.05, which differs appreciably from both α_1 and α_2.

In our previous publications [20,21], it has been shown that similar discrepancies have been found in Kapton and even more fragrant behavior has been observed in polyethylene terephthalate (PET) or polyethylene naphthalate (PEN). It is to reconcile pulsed and continuous irradiations in these commercial polymers that the RFVm model has been proposed in [20]. Nevertheless, there exists a group of polymers (photoconductive polyvinylcarbazole and molecularly doped polymers) including an ordinary polymer (low density polyethylene) that strictly follow the above RFV requirements [20]. Polymer assignment to the RFV or RFVm model depends critically on the comparison of pulsed and continuous irradiations under the conditions outlined above.

Future numerical work with the RFVm model analogous to that already done with the RFV model (see [18]) is highly needed to elaborate procedures producing one-valued model parameters with a clear physical meaning.

5. Conclusions

The combined pulsed and continuous irradiations of polyimide films (trademark PM-1) show that the conventional RFV model fails to describe RIC results consistently. For this purpose, we used the modified RFVm model proposed recently in our paper [20]. It replaces a simple exponential trap distribution of the conventional RFV model with an aggregate two-exponential one. This modification should not be confused with a two-trap model (now a model of choice in spacecraft charging community) with both traps having fixed energies. Finding the model parameters that fit the obtained RIC results was assisted by numerical calculations. A tentative set of the RFVm model parameters describing experimental data is proposed. Future work is needed to improve the accuracy of retrieving model parameters from the experiment, due to the discovered interconnection of the RFVm parameters requiring an application of the trial and error method that is contrary to a much more straightforward parameter selection of the conventional RFV model.

Our detailed analysis of the measuring method used to find the RIC in a polyimide PM-1 and develop the RFVm shows the importance of the proper accounting of the radiation-driven current and the RIC prompt component mostly overlooked in current investigations.

Author Contributions: A.T. and V.S. conceived, designed, and performed the experiments; A.Z. made all numerical calculations, prepared figures, and analyzed the data; E.P. was responsible for original draft preparation while A.T. reviewed and edited the text; project administration was performed by E.P.

Funding: This research received no external funding.

Acknowledgments: The authors would to thank R. Sh. Ikhsanov for help with numerical calculations. Support from the Basic Research Program of the National Research University Higher School of Economics is gratefully acknowledged.

Conflicts of Interest: The authors declare no conflict of interest.

References

1. Fowler, J.F. X-ray induced conductivity in insulating materials. *R. Soc. Lond.* **1956**, *150*, 464–480. [CrossRef]
2. Rose, A. An outline of photoconductivity in semiconductors. *RCA Rev.* **1951**, *12*, 362–414.
3. Arkhipov, V.I.; Iovu, M.S.; Rudenko, A.I.; Shutov, S.D. An analysis of the dispersive charge transport in vitrous 0.55 As_2Se_3. *Phys. Status Solidi* **1979**, *45*, 67–77. [CrossRef]
4. Tiedje, T.; Rose, A. A physical interpretation of dispersive transport in disordered semiconductors. *Solid State Commun.* **1981**, *37*, 49–52. [CrossRef]

5. Pope, M.; Swenberg, C.E. *Electronic Processes in Organic Crystals and Polymers*; Oxford University Press: New York, NY, USA, 1999; p. 1360.
6. Gross, B. Radiation-induced charge storage and polarization effects. In *Electrets*; Sessler, G.M., Ed.; Springer: Berlin, Germany; New York, NY, USA, 1980; pp. 217–284.
7. Tyutnev, A.P.; Saenko, V.S.; Pozhidaev, E.D.; Kolesnikov, V.A. Charge carrier transport in polyvinylcarbazole. *J. Phys. Condens. Matter* **2006**, *18*, 6365–6377. [CrossRef]
8. Tyutnev, A.P.; Weiss, D.S.; Dunlap, D.H.; Saenko, V.S. Time-of-flight current shapes in molecularly doped polymers: Effects of sample thicknessand irradiation side and carrier generation width. *J. Phys. Chem. C* **2014**, *118*, 5150–5158. [CrossRef]
9. Tyutnev, A.P.; Saenko, V.S.; Pozhidaev, E.D.; Akkerman, A.F. Transient radiation-induced conductivity in polymers. *Phys. Status Solidi A* **1982**, *73*, 81–89. [CrossRef]
10. Mingaleev, G.S.; Tyutnev, A.P.; Gerasimov, B.P.; Kulchitskaya, I.A. Numerical analysis of the transient radiation-induced conductivity in the framework of the Rose-Fowler-Vaisberg formalism. *Phys. Status Solidi A* **1986**, *93*, 251–262. [CrossRef]
11. Ikhsanov, R.S.; Tyutnev, A.P.; Saenko, V.S.; Pozhidaev, E.D. Analysis of dispersive carrier transport based on numerical solution of multiple trapping equations. *Polym. Sci. A* **2009**, *51*, 1032–1039. [CrossRef]
12. Arkhipov, V.I. An adiabatic model of trap-controlled dispersive transport and recombination. *J. Non-Cryst. Solids* **1993**, *163*, 274–282. [CrossRef]
13. Gross, B.; von Seggern, H.; Berkley, D.A. Long term behavior of radiation-induced currents in fluorinated ethylene propylene copolymer. *Phys. Status Solidi A* **1983**, *79*, 607–615. [CrossRef]
14. Faria, F.M.; Gross, B.; Filho, R.G. Radiation-induced conductivity of polymers in different gases. *J. Appl. Phys.* **1987**, *62*, 1420–1424. [CrossRef]
15. Hanna, R.; Paulmier, T.; Molinie, P.; Belhaj, M.; Dirassen, B.; Payan, D.; Balcon, N. Radustion-induced conductivity in space dialectric materials. *J. Appl. Phys.* **2014**, *115*, 033713. [CrossRef]
16. Gross, B.; Sessler, G.M.; West, J.E. Charge dynamics for electron-irradiated polymer-foil electrets. *J. Appl. Phys.* **1974**, *45*, 2841–2851. [CrossRef]
17. Gross, B.; Giacometti, J.A.; Ferreira, G.F.L. Charge storage and transport in electron-irradiated and corona-charged dielectrics. *IEEE Trans. Nucl. Sci.* **1981**, *28*, 4513–4522. [CrossRef]
18. Tyutnev, A.P.; Saenko, V.S.; Pozhidaev, E.D.; Ikhsanov, R.S. Experimental and theoretical studies of radiation-induced conductivity in spacecraft polymers. *IEEE Trans. Plasma Sci.* **2015**, *43*, 2915–2924. [CrossRef]
19. Kurtz, S.R.; Hughes, R.C. Radiation-induced photoconductivity in polymers: Polyvinylfluoride compared with polyethylene terephthalate. *J. Appl. Phys.* **1983**, *54*, 229–237. [CrossRef]
20. Tyutnev, A.P.; Saenko, V.S.; Ikhsanov, R.S.; Krouk, E.A. Radiation-induced conductivity in polymers under pulsed and long-time small-signal irradiations combined to determine their step-function response. *J. Appl. Phys.* **2019**, *126*, 095501. [CrossRef]
21. Tyutnev, A.P.; Saenko, V.S.; Zhadov, A.D.; Pozhidaev, E.D. Radiation-induced conductivity in Kapton-like polymers featuring conductivity rising with an accumulating dose. *IEEE Trans. Plasma Sci.* **2019**, *47*, 3739–3745. [CrossRef]
22. Beecken, B.P.; Englund, J.T.; Lake, J.J.; Wallin, B.M. Application of AF-NUMIT2 to the modeling of deep-dielectric spacecraft charging in the space environment. *IEEE Trans. Plasma Sci.* **2015**, *43*, 2817–2827. [CrossRef]
23. Hummel, A. Ionization in Nonpolar Molecular Liquids by High Energy Electrons. *Adv. Rad. Chem.* **1974**, *4*, 1–102.
24. van Lint, V.A.J. Mechanisms of transient radiation effects. *IEEE Trans. Nucl. Sci.* **1963**, *10*, 11–27. [CrossRef]
25. Compton, D.M.J.; Cheney, G.T.; Poll, R.A. Radiation induced conductivity in plastic films at high dose rates. *J. Appl. Phys.* **1965**, *36*, 2434–2443. [CrossRef]
26. van Lint, V.A.J.; Harrity, J.W.; Flanagan, T.M. Scaling laws for irradiation effects in insulators. *IEEE Trans. Nucl. Sci.* **1968**, *15*, 194–204. [CrossRef]
27. Ahrens., T.J.; Wooten., F. Electrical conductivity induced in insulators by pulsed radiation. *IEEE Trans. Nucl. Sci.* **1976**, *13*, 1268–1272. [CrossRef]
28. Tyutnev, A.P.; Abramov, V.N.; Dubenskov, P.I.; Saenko, V.S.; Vannikov, A.V.; Pozhidaev, E.D. Time-resolved nanosecond radiation-induced conductivity in polymers. *Acta Polym.* **1986**, *37*, 336–342. [CrossRef]

29. Williams, F. Kinetics of ionic processes in the radiolysis of liquid cyclohexane. *J. Am. Chem. Soc.* **1964**, *86*, 3954–3957. [CrossRef]
30. Tyutnev, A.P.; Ikhsanov, R.S.; Saenko, V.S.; Pozhidaev, E.D. A theoretical description of geminate recombination in polymers in the approximation of probability of survival of ionic pairs. *Russ. J. Phys. Chem. B* **2007**, *1*, 661–669. [CrossRef]
31. Ikhsanov, R.S.; Tyutnev, A.P.; Saenko, V.S.; Pozhidaev, E.D. A theoretical description of geminal electrical conductivity in polymers in the approximation of isolated ion pairs on the basis of solution of the Smoluchowski equation. *Russ. J. Phys. Chem. B* **2008**, *2*, 309–314. [CrossRef]
32. Tyutnev, A.P.; Saenko, V.S.; Karpechin, A.I.; Mingaleev, G.S.; Arkhipov, V.I.; Rudenko, A.I.; Vannikov, A.V. Radiation-induced conductivity in polymers under continuous irradiation. *Phys. Status Solidi A* **1984**, *83*, 365–373. [CrossRef]
33. Gross., B.; Faria, R.M.; Ferreira, G.F.L. Radiation-induced conductivity in Teflon irradiated by X-rays. *J. Appl. Phys.* **1981**, *52*, 571–577. [CrossRef]
34. Filho, R.G.; Gross, B. Time-resolved x-ray conductivity in polyethyleneterephthalate. *J. Appl. Phys.* **1989**, *68*, 5478–5483. [CrossRef]
35. Tyutnev, A.P.; Karpechin, A.I.; Boev, S.G.; Saenko, V.S.; Pozhidaev, E.D. Current overshoot in polymers under continuous irradiation. *Phys. Status Solidi A* **1992**, *132*, 3163–3170. [CrossRef]
36. Tyutnev, A.P.; Saenko, V.S.; Smirnov, I.A.; Pozhidaev, E.D. Radiation-induced conductivity in polymers during long-term irradiation. *High Energy Chem.* **2006**, *40*, 319–330. [CrossRef]
37. Molinie, P.; Dessante, P.; Hanna, R.; Paulmier, T.; Dirassen, B.; Belhaj, M.; Payan, D.; Balcon, N. Polyimide and FEP charging behavior under multienergetic electron-beam irradiation. *IEEE Trans. Dielectr. Electr. Insul.* **2012**, *19*, 1215–1220. [CrossRef]
38. Paulmier, T.; Dirassen, B.; Payan, D.; Arnaout, M. Analysis of charge transport and ionization effect in space used polymers under high energy electron irradiation. *IEEE Trans. Plasma Sci.* **2017**, *45*, 1933–1937. [CrossRef]
39. Pacaud, R.; Paulmier, T.; Sarrailh, P. 1-D physical model of charge distribution and transport in dielectric materials under space radiations. *IEEE Trans. Plasma Sci.* **2017**, *45*, 1933–1937. [CrossRef]
40. Mateo-Velez, L.-C.; Paulmier, T.; Sicard, A.; Dirrassen, B.; Payan, D. Experimental investigation of surface potentials of materials under electron spectra representative of GEO and MEO worst case environments. *IEEE Trans. Plasma Sci.* **2019**, *47*, 3885–3890. [CrossRef]
41. Sessler, G.M.; Figueiredo, M.T.; Ferreira, G.F.L. Models of charge transport in electron-beam irradiated insulators. *IEEE Trans. Dielectr. Electr. Insul.* **2004**, *11*, 192–202. [CrossRef]
42. Sadovnichii, D.N.; Tyutnev, A.P.; Milekhin, Y.M. Bulk charging of polymer films under electron irradiation. In Proceedings of the 9th International Symposium on Materials in a Space Environment, Noordwijk, The Netherlands, 16–20 June 2003.
43. Khatipov, S.A. Radiation-induced electron transport processes in polymeric dielectrics (a review). *High Energy Chem.* **2001**, *35*, 291–307. [CrossRef]
44. Tyutnev, A.P.; Sadovnichii, D.N.; Saenko, V.S.; Pozhidaev, E.D. The effect of molecular motions on the transport of excess charge carriers in polymers. *Polym. Sci. A* **2000**, *42*, 10–18.
45. Tyutnev, A.P.; Weiss, D.S.; Saenko, V.S.; Pozhidaev, E.D. About mobility thickness dependence in molecularly doped polymers. *Chem. Phys.* **2017**, *495*, 16–22. [CrossRef]
46. Tyutnev, A.P.; Ikhsanov, R.S.; Saenko, V.S.; Nikerov, D.V. Numerical analysis of the photo-injection time-of-flight curves in molecularly doped polymers. *Chem. Phys.* **2018**, *503*, 65–70. [CrossRef]